Published in final edited form as:
IEEE Trans Med Imaging. 2009 September ; 28(9): 1459–1467. doi:10.1109/TMI.2009.2017741.

Impact on Reader Performance for Lesion-Detection/Localization Tasks of Anatomical Priors in SPECT Reconstruction

Andre Lehovich [Member, IEEE],
Division of Nuclear Medicine, Department of Radiology, University of Massachusetts Medical School, Worcester, MA 01655 USA

Philippe P. Bruyant,
FRV Sciences, 29820 Guilers, France

Howard S. Gifford [Member, IEEE],
Division of Nuclear Medicine, Department of Radiology, University of Massachusetts Medical School, Worcester, MA 01655 USA

Peter B. Schneider,
Division of Nuclear Medicine, Department of Radiology, University of Massachusetts Medical School, Worcester, MA 01655 USA

Shayne Squires,
Division of Nuclear Medicine, Department of Radiology, University of Massachusetts Medical School, Worcester, MA 01655 USA

Robert Licho,
Division of Nuclear Medicine, Department of Radiology, University of Massachusetts Medical School, Worcester, MA 01655 USA

Gene Gindi [Senior Member, IEEE], and
Department of Radiology, State University of New York (SUNY), Stony Brook, NY 11794 USA

Michael A. King [Senior Member, IEEE]
Division of Nuclear Medicine, Department of Radiology, University of Massachusetts Medical School, Worcester, MA 01655 USA

Andre Lehovich: andre.lehovich@umassmed.edu; Philippe P. Bruyant: philippe.bruyant@frvsciences.fr; Howard S. Gifford: howard.gifford@umassmed.edu; Peter B. Schneider: peter.schneider@umassmed.edu; Shayne Squires: squiress@ummhc.org; Robert Licho: lichor@ummhc.org; Gene Gindi: gindi@mil.sunysb.edu; Michael A. King: michael.king@umassmed.edu

Abstract

With increasing availability of multimodality imaging systems, high-resolution anatomical images can be used to guide the reconstruction of emission tomography studies. By measuring reader performance on a lesion detection task, this study investigates the improvement in image-quality due to use of prior anatomical knowledge, for example organ or lesion boundaries, during SPECT reconstruction. Simulated ^{67}Ga-citrate source and attenuation distributions were created from the mathematical cardiac-torso (MCAT) anthropomorphic digital phantom. The SIMIND Monte Carlo software was then used to generate SPECT projection data. The data were reconstructed using the De Pierro maximum a posteriori (MAP) algorithm and the rescaled-block-iterative (RBI) algorithm for comparison. We compared several degrees of prior knowledge about the anatomy: no knowledge about the anatomy; knowledge of organ boundaries; knowledge of organ and lesion boundaries; and knowledge of organ, lesion, and pseudo-lesion (non-emission uptake altering)

Correspondence to: Andre Lehovich, andre.lehovich@umassmed.edu.

boundaries. The MAP reconstructions used quadratic smoothing within anatomical regions, but not across any provided region boundaries. The reconstructed images were read by human observers searching for lesions in a localization receiver operating characteristic (LROC) study of the relative detection/localization accuracies of the reconstruction algorithms. Area under the LROC curve was computed for each algorithm as the comparison metric. We also had humans read images reconstructed using different prior strengths to determine the optimal trade-off between data consistency and the anatomical prior. Finally by mixing together images reconstructed with and without the prior, we tested to see if having an anatomical prior only some of the time changes the observer's detection/localization accuracy on lesions where no boundary prior is available. We found that anatomical priors including organ and lesion boundaries improve observer performance on the lesion detection/localization task. Use of just organ bound aries did not provide a statistically significant improvement in performance however. We also found that optimal prior strength depends on the level of anatomical knowledge, with a broad plateau in which observer performance is near optimal. We found no evidence that having anatomical priors use lesion boundaries only when available changes the observer's performance when they are not available. We conclude that use of anatomical priors with organ and lesion boundaries improves reader performance on a lesion-detection/localization task, and that pseudo-lesion boundaries do not hurt reader performance. However, we did not find evidence that a prior using only organ boundaries helps observer performance. Therefore we suggest prior strength should be tuned to the organ-only case, since a prior will likely not be available for all lesions.

Index Terms

Anatomical priors; localization receiver operating characteristic (LROC); reader performance; SPECT image reconstruction

I. Introduction

Dual-modality imaging systems are coming into widespread clinical use and remain an important research area. Such systems combine a functional modality such as SPECT or positron emission tomography (PET) with a high-resolution anatomical modality such as computed tomography (CT) or magnetic resonance imaging (MRI) [1]–[5]. These systems provide anatomical images which are coregistered to the functional images, and can be used to estimate attenuation maps for use in attenuation correction of the emission acquisitions. The coregistration of the anatomical and emission studies also allows for the use of anatomical slices as prior knowledge which can be integrated into emission reconstruction [6]–[8]. Assessment of the potential utility of employing these aligned anatomical modalities to produce anatomical priors for emission reconstruction is of significant interest given the current clinical availability of such systems. Objective assessment of reconstruction strategies intended for clinical usage is best performed with tasks modeled on those employed clinically. Generally such tasks can be divided into estimation (quantification) and classification (detection) [9]. An assessment of the utility of anatomical priors in terms of a combined detection/localization task was the aim of our investigations. In a detection/localization task the observer must decide if an image contains a lesion and identify the most likely lesion location.

Much of the previous work on task-based assessment of anatomical priors in emission-tomography reconstruction has focused on quantification. For example, Comtat *et al.* [10] showed that the use of blurred anatomical labels in 3-D PET reconstruction improved reconstructed slices as assessed by using region-of-interest (ROI) figures-of-merit (FOMs) such as the mean estimated bias, standard deviation, and RMS error. They noted an improvement in noise-bias trade-offs which was more evident for larger objects. They also

investigated what happens when pseudo-lesions are present. Pseudo-lesions are anatomical lesions which do not have a corresponding change in the activity distribution. In their study pseudo-lesions increased the variance but did not alter the bias. This led them to hypothesize that pseudo-lesions could result in false-positives for detection tasks. More recently Alessio and Kinahan determined that use of anatomical priors improved the quantification of activity in tumors of various sizes and activity levels in terms of bias and variance [11].

A limited number of studies have been performed assessing the impact of anatomical priors on the classification task [12]–[15]. Comparison between studies is difficult due to differences in, among other things, the task (detection, localization, or detection/localization), the observer (numerical or human), imaging modality (SPECT or PET), and complexity of the images employed [13]. Nuyts *et al.* [12] observed with simulated fluorodeoxyglucose (FDG) PET brain imaging that the use of an anatomical prior in maximum a posteriori (MAP) reconstruction yielded better performance in terms of detection accuracy of reduced-count lesions than postsmoothing of maximum-likelihood expectation-maximization (MLEM) reconstructions. They assessed performance using the channelized-Hotelling observer (CHO) performing the signal-known-exactly--background-known-exactly (SKE-BKE) task.

A recent investigation by Kulkarni *et al.* [13] used the CHO to analyze lesion detection accuracy in simulated abdominal SPECT slices of MAP reconstruction employing anatomical priors versus not employing priors. They did not observe any benefit from use of a prior that included organ or organ plus lesion boundaries for the task of detecting a signal at a known location. However, they did not investigate the effect of degree of proximity of the lesion to an organ for a lesion search task. Baete *et al.* [14] observed a statistically significant improvement in lesion localization in simulated FDG-PET brain images by six physicians performing a multiple-alternative forced-choice (M-AFC) paradigm when anatomical information was included in MAP reconstruction as opposed to postsmoothing of maximum-likelihood expectation-maximization (MLEM) slices.

We have employed the performance of the combined detection/localization task in simulated ^{67}Ga-Citrate SPECT imaging for mediastinal lymphoma to evaluate choices for filtering [16], the inclusion of attenuation correction [17], the modeling of distance-dependent spatial resolution [18], and scatter correction [19]. These investigations were extended by Bruyant *et al.* [15] to include an evaluation of the use of anatomical priors in MAP reconstruction using a version of the CHO with localization (LROC CHO). They found that using boundaries of organs and lesions to control smoothing in MAP reconstruction improved performance compared to the rescaled block-iterative (RBI) algorithm with no prior [20]. The comparison was conducted using simulated ^{67}Ga-Citrate thorax projections, but did not include Compton scatter in the simulation. No benefit was observed for the anatomical prior using solely organ boundaries, although motivation for a benefit was postulated. Generally the inclusion of pseudo-lesions did not significantly alter the improvement in detection/localization accuracy.

Herein we report on the extension of the above investigation of Bruyant *et al.* [15] to simulated ^{67}Ga-Citrate imaging when scatter is included in the projections, and scatter correction is included in reconstruction. We perform a human-observer comparison of the use of MAP reconstruction employing anatomical priors to MAP reconstruction without the use of priors and RBI reconstruction with post-smoothing. These human-observer studies were performed using the localization receiver operating characteristic (LROC) paradigm [21] where the observer provides the site of the suspected lesion and a confidence rating. Both MAP reconstruction without the use of priors and RBI reconstruction were previously optimized using the combined detection/localization task for the class of images investigated

herein [20], [22]. The selection of the strength of the anatomical prior in MAP reconstruction was also previously optimized by use of the LROC CHO [23]. However, we include a human-observer evaluation of the impact of prior strength to further examine the selection employed in the comparison study. We also explore whether the use of lesion boundaries in anatomical priors only some of the time impacts human-observer performance when the boundaries are not available. Although the focus of this study is for SPECT/CT we believe it also gives insight into SPECT/MRI, PET/CT, and PET/MRI.

II. Materials and Methods

A. Data Simulation

Data simulation followed previously reported techniques [19]. Briefly, we used the 3-D mathematical cardiac-torso (MCAT) anthropomorphic digital phantom [24] to create the background (lesion-free) distribution of ^{67} Ga Citrate in lymphoma imaging. The distribution of Gallium within this phantom was based on postmortem examinations of human subjects [25]. Adjustment in bone marrow uptake was made in consultation with the clinicians in our department so that the reconstructed slices more closely matched the appearance of clinical ^{67}Ga-Citrate studies. The simulated source and attenuation distributions were 256 × 256 × 256 voxels with size 1.585 mm.

The SIMIND Monte Carlo program [26] was used to generate simulated noise-free projection images from this background radiotracer distribution, as imaged by a medium-energy general-all-purpose (MEGAP) parallel-hole collimator with a system spatial resolution of 10.5 mm at 10 cm from its face. The simulation included the effects of attenuation, Compton scatter, and distance-dependent spatial resolution. Separate projections were created for the 15% photopeak centered at 93 keV and 185 keV and for adjacent 8 keV scatter windows around each photopeak [19]. The photopeak windows were combined prior to reconstruction. The contributions of the complete emission spectrum of ^{67}Ga were included in simulation. A total of 450 × 10^6 photons from all photopeak emission energies were collected at each projection angle, resulting in an estimate of the noise-free projection data. The 93- and 185-keV projections were weighted by their emission abundances and by the camera efficiency as suggested in [27], summed, and then collapsed into 128 × 128 projections at 120 different projection angles encompassing 360° prior to reconstruction. The size of the projection pixels and reconstructed voxels is therefore 3.170 mm.

Spherical, 1-cm-diameter lesions were then placed at each of 300 different possible lesion locations throughout the mediastinal region of the phantom. For each location the noise-free lesion projection data was simulated with Monte Carlo in a manner identical to that described for the background. We used 1 cm lesions because these are the smallest that would be found abnormal on a CT scan. Possible lesion locations were chosen under consultation of a physician and were placed in clinically likely locations. The lesions were added to the background projections to generate the mean lesion-present phantom projections.

A range of lesion-contrast ratios were chosen to make the task more realistic than with only a single lesion contrast. Because of the partial-volume effect, small changes in lesion size will manifest themselves as changes in contrast rather than the size of the reconstructed lesion [17]. Based on the results of an unpublished pilot reader study we selected lesion:background ratios of 25:1, 27.5:1, and 30:1, with one third of the lesions at each contrast. Our experience in past studies using RBI has been these contrasts give a mix of lesions ranging from fairly easy to fairly difficult. When reconstructing with RBI this resulted in areas under the LROC curve of 0.61, 0.63, and 0.68, respectively, giving observers a range of difficulties.

Each lesion-present volume included six lesions located at different levels of the torso, with at least three slices between lesions. Before reconstruction of the 120 noise-free photopeak projections, Poisson noise was added such that the total number of counts was 14.8 million. This produces a noise level comparable to that seen in acquisitions at our clinic.

B. Image Reconstruction

Each of the simulated data sets was reconstructed using five 3-D reconstruction strategies. As a baseline control we used the rescaled block-iterative (RBI) algorithm [28] for four iterations (30 subsets with four projections each), and then smoothed with a Gaussian filter (σ = 1.274 pixels). These reconstruction parameters were selected because they maximized performance in previous model- and human-observer studies [20]. We also computed four different smoothing strategies for MAP reconstruction, using the De Pierro algorithm [29] as described below; the parameters for these reconstructions were optimized using the LROC CHO and limited human-observer studies [20], [23]. All reconstructions used triple-energy window (TEW) scatter correction [30] applied within reconstruction [31]. The system matrix used for reconstruction included the effects of depth-dependent collimator blur and attenuation [18].

MAP reconstruction makes a tradeoff between enforcing data consistency, measured using the log-likelihood, and consistency with prior knowledge [32]. The tradeoff is controlled by the prior strength β; larger values of β weight prior knowledge more heavily. When β is zero no prior knowledge is used, giving a maximum-likelihood solution. When β is infinity the data is ignored in favor of the prior. The MAP reconstruction $\widehat{\vec{f}}_{\text{map}}$ is defined by

$$\widehat{\vec{f}}_{\text{map}} = \arg\max_{\vec{f}} \left[\log\left(\text{likelihood}(\vec{f})\right) + \beta \text{logprior}(\vec{f}) \right]. \quad (1)$$

Our likelihood model assumes gamma rays are emitted from each voxel according to a Poisson distribution. We use convex quadratic priors similar to those used by [10] and [13]. Full implementation details are described in [23]. Briefly, these priors smooth within anatomical regions, but not across boundaries. Each prior is computed by summing over voxels

$$\beta \text{logprior}(\vec{f}) = \beta \sum_i \text{prior}_i. \quad (2)$$

The prior term for voxel i is defined by

$$\text{prior}_i = \frac{1}{2} \sum_{n \in N_i} \frac{1}{\text{dist}(i,n)} (f_i - f_n)^2 \quad (3)$$

where N_i is a set of the neighboring voxels around i, and dist(i, n) is the distance between the centers of voxels i and n. Knowledge about the anatomy, in the form of organ (and perhaps lesion) boundaries, is used to determine the voxels included in N_i. We use up to the 26 nearest neighbors in 3-D, but only those within same anatomical region. As a consequence of (3) the prior terms on each voxel are not independent.

The MAP reconstructions were computed using four different smoothing strategies of the above form, varying the amount of prior information about the anatomy used to determine

N_j. The first strategy (label "Q" for "quadratic") placed all voxels in the same region, and thus incorporated no anatomical information. This strategy always used all 26 nearest neighbors for N_j, regardless of anatomy.

The second strategy (label "O" for "organ") defined anatomical regions using information about organ boundaries, but had no knowledge about lesions. Only voxels on the same side of the boundary were included in N_j. This corresponds to the case in which organs can be seen in the high-resolution modality, but not lesions.

The third strategy (label "O+L" for "organ and lesion") had information about both the organ boundaries and, if and only if a lesion was present in the simulation, also the lesion boundary. This corresponds to the somewhat stylized situation where a radiotracer-avid lesion is always visible in the high-resolution anatomical-imaging modality.

The fourth strategy (label "O+P" for "organ and pseudo-lesion") had information about the organ boundaries and always had information about lesion boundaries, regardless of whether or not a lesion was present in the simulation. That is, lesion boundaries were present when lesions where included in the image, as per O+L, and were also included over non-lesion areas when no lesion was present. Such "pseudo-lesions" might occur when a necrotic region is visible in the high-resolution modality, but does not have increased radiotracer uptake. Each lesion-present case had a matching lesion-absent case. Thus the pseudo-lesions were added at the same location as true lesions.

A summary of the reconstruction strategies is found in Table I. All MAP reconstructions were computed using the De Pierro algorithm [29], run to approximate convergence in the following way: the first four iterations respectively used 4, 8, 24, and 60 projections per subset, followed by 50 iterations with 120 projections per subset.

C. Observer Studies

We extracted individual transverse slices from the 3-D reconstructions for analysis by human observers. All lesion-present and matching lesion-absent slices were through the center of a lesion location. To keep reading time to a reasonable length, each slice was read independently and surrounding slices were not shown to the observers, as providing the readers with 3-D information is not expected to make a large difference in the relative rankings of the reconstruction strategies [33]. We refer to one of these slices displayed to the readers as a case. We randomly selected half of the lesion locations to get 150 simulated lesion-present cases, and 150 matching lesion-absent cases. We partitioned the cases into 100 training cases and 200 study cases.

An upper threshold, above which all pixels were displayed as white, was applied to the reconstructed images to improve the lesion-to-background contrast, while leaving noise structure in the vicinity of the lesion unaffected. A separate threshold was determined for each of the different reconstruction strategies. Lesion-present and lesion absent slices had the same threshold. The lesion-pixel maximums were obtained for all of the image locations used in the study. The standard deviation σ of this set of maximums $\{S_{\max}\}$ was calculated and the upper threshold set to $\max\{S_{\max}\} + \sigma$. This threshold was chosen to increase lesion contrast but leave unaffected the noise structure in the region of the lesion. After thresholding the slices were interpolated to 256 × 256 pixels and quantized to 8 bits. The size of the final pixels is thus again 1.585 mm. Reconstructions of a sample case with the lesion located far away from organ boundaries are shown in Fig. 1. Reconstructions of a different case with the lesion located close to an organ boundary are shown in Fig. 2. The impact of prior strength β on the reconstruction is illustrated in Fig. 3.

Observer studies were conducted in a darkened room using a monitor with a perceptually-linearized grayscale [34]. The perceptual linearization resulted in a displayed image with 128 possible grayscale values. Ambient light was kept to a minimum by drawing a curtain across the reading-room door and turning off all light sources other than the monitor. A cardboard mask was used to hide extraneous parts of the screen. Observers were allowed to adjust the chair to be comfortable. For each case shown, the observers were asked to select the most likely lesion location via a movable cross-hair controlled by a computer mouse, and to provide a confidence rating that a lesion is present on scale ranging from one (confident, no lesion present) to six (confident, lesion present). During training observers were given feedback as to the truth regarding lesion presence and location after recording their confidence score. No feedback was supplied to the observer when reading the actual study cases. Only the ratings for the study slices were employed in the assessment of lesion detectability/localization.

We conducted three studies: a study to compare the different strategies and asses the impact of different types of prior anatomical knowledge, a study to find the optimal value of β, and a study to see if having priors present only some of the time hurts performance when they are no longer available.

1) Study to Compare Smoothing Strategies—Based on a preliminary study [23], two values of the smoothing parameter, $\beta = 0.005$ and $\beta = 0.04$, were chosen for reading by human observers. The readers were three scientists in our medical-physics research group and two physicians in our nuclear-medicine clinic. We began by having each reader read the 100 training cases reconstructed using each smoothing strategy. This was done in nine sessions, each consisting of cases reconstructed using one strategy (RBI, plus four MAP each at two values of β). Cases within a session were read in a random order, and the strategies were read in a random order. Thus all readers saw the same cases and strategies, but each in a different order.

After the initial training, we had the readers read the 200 study cases reconstructed by each strategy. The study cases were divided into 18 sessions of 100 images. Each session consisted of cases reconstructed using only one algorithm. No feedback was provided for any of the study cases. At the beginning of each session, the reader reread 50 training cases, again receiving feedback about the truth. Reading 50 training cases followed by 100 study cases takes about 20 min. The two sessions for each observer and reconstruction strategy were pooled, and area under the localization-response operating characteristic (LROC) curve was computed using Swensson's algorithm [21]. Swensson's algorithm uses a binormal model to fit an LROC curve to the observer's ratings. We tested for statistical significance using two-way ANOVA followed by Tukey's honestly significant differences (HSD) test [35].

2) Study to Optimize β—The LROC CHO and human-observer preliminary studies [23], [36] predicted there wouldn't be a large difference between $\beta = 0.005$ and $\beta = 0.04$. The just described study found a larger difference than expected in areas under the LROC curve (see results below), so we did a second study to better determine the optimal value of β. This study also consisted of 100 training cases and 200 study cases, though different cases were used than in the study to compare algorithms. The physicians did not participate in this study, nor in the mixing-priors study below; therefore there were only three readers. As these observers had already been through the study to compare algorithms, we did not include an initial training phase. However, as before, each session began with reading 50 retraining cases, followed by 100 study cases. Sessions consisted of cases reconstructed using $\beta \in \{0.02, 0.04, 0.06, 0.1, 0.2, 1.0\}$, and we again computed area under the LROC curve.

3) Mixing Priors Study—The study comparing reconstruction strategies found that using lesion boundaries in the prior makes the lesions easier to detect/localize (see results below). But in clinical practice such strong prior knowledge will only be available some of the time; for some patients we may not have a high-resolution anatomical scan, and other times such a scan will not show boundaries of all lesions. When the physician is searching for lesions, as is the case in this study, he/she may not know if the lesion boundary was included in the prior or not. It is possible that having the lesion prior present some of the time could change the observer's search strategy, and thus degrade performance when prior knowledge about the lesion is not available. To test this we did a study in which we mixed cases reconstructed with and without the lesion boundary in the prior.

This study again consisted of 100 training cases and 200 study cases. We took the reconstructions using prior O and prior O+L ($\beta = 0.04$) and mixed them together for reading. Readers received no information about whether or not the lesion boundary was used, other than what could be seen in the image. Then we unmixed the cases and scored each strategy separately. Control sessions, consisting of only one or the other prior, were also read and scored.

III. Results

A. Study to Compare Smoothing Strategies

Results for the five readers are shown in Fig. 4, where it can be seen that strategies O+L and O+P have higher areas under the LROC curve than the RBI baseline for both levels of the prior strength (β). Two-way ANOVA analysis confirmed a statistically significant difference exists between strategies ($p < 0.001$). Table II summarizes use of Tukey's HSD test to compare the detection/localization accuracy of the strategies. The test finds that strategies using the organ + lesion boundaries (O+L) and organ + lesion + pseudo-lesion boundaries (O+P) were significantly better than the RBI baseline for both prior strengths ($p < 0.05$). The same test found that for both the O+L and O+P strategies the stronger prior ($\beta = 0.04$) was significantly better than the weaker prior ($\beta = 0.005$) ($p < .05$). The Tukey-HSD test also found that at $\beta = 0.04$ O+L and O+P were significantly better than Q and O at either strength. No significant difference was observed between the strategy with no anatomical boundaries (Q) and the RBI baseline, confirming our previous observation that use of a nonanatomical quadratic prior did not improve LROC observer performance [20]. Similarly the strategy employing just the organ boundaries (O) also showed no significant difference to the RBI baseline, unlike what we had observed in previous LROC CHO studies when the projection images did not include scatter [23].

We partitioned the lesion locations into three sets: those close to organ boundaries, defined as less than five pixels (7.9 mm) from the nearest organ boundary (58 cases); those at medium distance, between five and eight pixels (between 7.9 mm and 12.7 mm) from organs (58 cases); and far lesions, further than eights pixels (12.7 mm) away from organ boundaries, (84 cases). This partitioning was done in the 2-D slices displayed to the readers. The area under the LROC curve for each observer/partition combination was then computed, together with the mean and standard deviation for each strategy, as shown in Fig. 5. The graph shows that, not surprisingly, lesions far from organ boundaries are easier to find than those close to organs. Inter-reader variability, indicated by the error bars, also increases when lesions are near organ boundaries.

We found that the including lesion boundaries in the prior improved observer performance when ($\beta = 0.04$, regardless of lesion location, however the effect is larger when lesions are close to the boundary, as suggested by [13]. For example, for close lesions RBI had a mean area of 0.44 ±0.11, and strategy sO+L was 0.69 ± 0.11, an improvement of 0.25, while for

far lesions RBI had an area of 0.88 ± 0.03 and strategy sO+L of 0.93 ± 0.03 (an improvement of 0.05).

B. Study to Optmize β

Plots showing observer performance as a function of prior strength are given in Fig. 6. For strategy O there is a plateau in the region $0.02 \leq \beta \leq 0.1$, followed by a pronounced dropoff as prior strength is increased past that point. Strategies O+L and O+P showed much less dependence on strength, with a peak somewhere between $0.1 < \beta < 1.0$. We did not extend this study to lower prior strengths, as we had already ascertained that $\beta = 0.04$ had higher performance than $\beta = 0.005$, and thus performance would drop off for lower strengths. (Note that the $\beta = 0.005$ points in Fig. 6 are reproduced from the previous study, and therefore are based on different cases than the other points.)

C. Mixing Priors Study

Table III gives results from the mixture study. In clinical practice lesion boundaries will only be available for use in a subset of patients. These results show that a mixture of cases reconstructed with and without lesion boundaries in the prior does not affect observer performance. This suggests that the availability of lesion boundaries does not change the observer's reading strategy, or alternatively that the reader recognizes when lesion boundaries are not available and is able to adjust reading strategy.

IV. Discussion

Providing the reading physician with access to coregistered images from both modalities has been shown to improve lesion localization [37], [38]. In this paper, we are considering a related question: does incorporating prior knowledge about the patient's anatomy, as could be derived from the high-spatial-resolution modality, into emission-tomography reconstruction improve reader accuracy for the lesion detection/localization task?

The results shown in Fig. 4 indicate that reconstructing with anatomical priors does improve performance for the LROC task when the prior includes boundaries for the lesion plus organs, but not organ boundaries alone. Thus, to see useful gains one must include lesion boundaries in the prior. (Note that this only requires the boundaries be obtainable from the high-resolution modality in an automated fashion, not that a human must go in and specify the lesion boundary.) We have not investigated a strategy that uses lesion boundaries without organ boundaries, as in clinical practice this will not always be possible, furthermore for any given patient one likely would not know if lesion boundaries were available. Because we found optimal prior strength for the strategy with lesion boundaries is in the region where observer performance for the only-organ strategy is rapidly dropping off (see Fig. 6), we suggest prior strength should be tuned to the case without lesion boundaries.

Other researchers have suggested that including boundaries for regions that do not have increased uptake (pseudo-lesions) in the prior might have a detrimental affect on image quality [10], [13]. We did not find any evidence in this study that pseudo-lesions impact observer performance.

Our results differ somewhat from several prior studies. For example Nuyts *et al.* [12] reported that anatomical priors improve lesion detectability, even without including lesion boundaries. Their study differed from ours in several important respects. First, they investigated application to PET brain imaging, whereas we are investigating SPECT ^{67}Ga tumor imaging. Second, they made use of prior knowledge about the level of activity expected in different anatomical regions, whereas strategies we investigated do not. As a result their prior had a different functional form than the convex quadratic priors we used.

Third, their lesions were cold spots with reduced activity, while ours are hot spots. Finally, their detection task was for a known signal at a known location, with no search.

On the other hand, Kulkarni *et al.* [13] found that anatomical priors, even those including lesion boundaries, do not improve lesion detectability for SPECT imaging. They used the same convex quadratic prior functional form that we used. They assumed a known lesion at a known location, and did not include search in their detection task, which was performed by a CHO. Therefore, their lesions were of much lower intensity than ours. They found that a prior using lesion boundaries could turn noise correlations into a false-positive or false-negative lesion. For our brighter lesions this effect does not seem to occur with human observers.

We used a quadratic prior, although other functional forms for the prior are being actively researched [39]–[41]. It is possible that using a different functional form for the prior might improve performance when lesion boundaries are not available, as was found in [39].

In this work, we have not given the readers access to high-resolution anatomical images, such as those from the CT half of a SPECT/CT or PET/CT system. It is, therefore, possible that we have overstated the impact of anatomical priors. We will be investigating this in a future study.

V. Conclusion

We determined that incorporating anatomical boundaries as prior knowledge in SPECT reconstruction can improve observer performance. Using a convex quadratic prior, we found lesion boundaries needed to be included to achieve a statistically significant improvement for the detection/localization task. However, performance, measured by area under the LROC curve, drops off more quickly as a function of prior strength β when only organ boundaries are used than when organ and lesion boundaries are used. Therefore, prior strength should be tuned to the case where only organ boundaries are known, as it is likely that some lesions will only be visible with SPECT but not the higher-resolution anatomical modality. Including boundaries of pseudo lesions in the prior did not hurt observer performance. We found no evidence that including lesion boundaries in the prior only some of the time hurt observer performance when they were not available.

Acknowledgments

The authors would like to thank an anonymous referee of our grant renewal for suggesting the mixture study.

This work was supported by National Institute of Biomedical Imaging and Bioengineering under Grant RO1 EB002798. This work was reported in part at the 2006 and 2007 IEEE Medical Imaging Conferences and in the accompanying proceedings. The contents are solely the responsibility of the authors and do not necessarily represent the official views of the National Institutes of Health.

References

1. Beyer T, Townsend DW, Brun T, Kinahan PE, Charron M, Roddy R, Jerin J, Young J, Byars L, Nutt R. A combined PET/CT scanner for clinical oncology. J Nucl Med. Aug; 2000 41(8):1369–1379. [PubMed: 10945530]
2. Hany TF, Steinert HC, Goerres GW, Buck A, von Schulthess GK. PET diagnostic accuracy: Improvement with in-line PET-CT system: Initial results. Radiol. Nov; 2002 225(2):575–581.
3. Lang TF, Hasegawa BH, Liew SC, Brown JK, Blankespoor SC, Reilly SM, Gingold EL, Cann CE. Description of a prototype emission-transmission computed tomography imaging system. J Nucl Med. Oct; 1992 33(10):1881–1887. [PubMed: 1403162]

4. Zaidi H, Montandon ML, Slosman DO. Magnetic resonance imaging-guided attenuation and scatter corrections in three-dimensional brain positron emission tomography. Med Phys. May; 2003 30(5): 937–948. [PubMed: 12773003]
5. Catana C, Wu Y, Judenhofer MS, Qi J, Pichler BJ, Cherry SR. Simultaneous acquisition of multislice PET and MR images: Initial results with a MR-compatible PET scanner. J Nucl Med. Dec; 2006 47(12):1968–1976. [PubMed: 17138739]
6. Johnson V, Wong W, Hu X, Chen C. Image restoration using Gibbs priors: Boundary modeling, treatment of blurring, and selection of hyperparameter. IEEE Trans Pattern Anal Mach Intell. May; 1991 13(5):413–425.
7. Gindi G, Lee M, Rangarajan A, Zubal IG. Bayesian reconstruction of functional images using anatomical information as priors. IEEE Trans Med Imag. Dec; 1993 12(4):670–680.
8. Bowsher JE, Johnson VE, Turkington TG, Jaszczak RJ, Floyd CE Jr, Coleman RE. Bayesian reconstruction and use of anatomical a priori information for emission tomography. IEEE Trans Med Imag. Oct; 1996 15(5):673–686.
9. Barrett HH. Objective assessment of image quality: Effects of quantum noise and object variability. J Opt Soc Am A Opt Image Sci Vis. Jul; 1990 7(7):1266–1278.
10. Comtat C, Kinahan PE, Fessler JA, Beyer T, Townsend DW, Defrise M, Michel C. Clinically feasible reconstruction of 3-D whole-body PET/CT data using blurred anatomical labels. Phys Med Biol. Jan; 2002 47(1):1–20. [PubMed: 11814220]
11. Alessio AM, Kinahan PE. Improved quantitation for PET/CT image reconstruction with system modeling and anatomical priors. Med Phys. Nov; 2006 33(11):4095–4103. [PubMed: 17153389]
12. Nuyts J, Baete K, Bequé D, Dupont P. Comparison between MAP and postprocessed ML for image reconstruction in emission tomography when anatomical knowledge is available. IEEE Trans Med Imag. May; 2005 24(5):667–675.
13. Kulkarni S, Khurd P, Hsiao I, Zhou L, Gindi G. A channelized Hotelling observer study of lesion detection in SPECT MAP reconstruction using anatomical priors. Phys Med Biol. Jun; 2007 52(12):3601–3617. [PubMed: 17664562]
14. Baete K, Nuyts J, Laere KV, Paesschen WV, Ceyssens S, Ceuninck LD, Gheysens O, Kelles A, den Eynden JV, Suetens P, Dupont P. Evaluation of anatomy based reconstruction for partial volume correction in brain FDG-PET. Neuroimage. Sep; 2004 23(1):305–317. [PubMed: 15325378]
15. Bruyant PP, Gifford HC, Gindi G, King MA. Numerical observer study of MAP-OSEM regularization methods with anatomical priors for lesion detection in ^{67} Ga images. IEEE Trans Nucl Sci. Feb; 2004 51(1):193–197.
16. Wells RG, Simkin PH, Judy PF, King MA, Pretorius PH, Gifford HC. Effect of filtering on the detection and localization of small Ga-67 lesions in thoracic single photon emission computed tomography images. Med Phys. Jul; 1999 26(7):1382–1388. [PubMed: 10435542]
17. Wells RG, King MA, Simkin PH, Judy PF, Brill AB, Gifford HC, Licho R, Pretorius PH, Schneider PB, Seldin DW. Comparing filtered backprojection and ordered-subsets expectation maximization for small-lesion detection and localization in ^{67}Ga SPECT. J Nucl Med. Aug; 2000 41(8):1391–1399. [PubMed: 10945533]
18. Gifford HC, King MA, Wells RG, Hawkins WG, Narayanan MV, Pretorius PH. LROC analysis of detector-response compensation in SPECT. IEEE Trans Med Imag. May; 2000 19(5):463–473.
19. Farncombe TH, Gifford HC, Narayanan MV, Pretorius PH, Frey EC, King MA. Assessment of scatter compensation strategies for ^{67}Ga SPECT using numerical observers and human LROC studies. J Nucl Med. May; 2004 45(5):802–812. [PubMed: 15136630]
20. Gifford HC, King MA, Narayanan MV, Pretorius PH, Smyczynski MS. Effect of block-iterative acceleration on Ga-67 tumor detection in thoracic SPECT. IEEE Trans Nucl Sci. Feb; 2002 49(1): 50–55.
21. Swensson RG. Unified measurement of observer performance in detecting and localizing target objects on images. Med Phys. Oct; 1996 23(10):1709–1725. [PubMed: 8946368]
22. Gifford, HC.; Pretorius, PH.; King, MA. Comparison of human-and model-observer LROC studies. In: Chakraborty, DP.; Krupinski, EA., editors. Proc SPIE Med Imag 2003: Image Perception, Observer Performance, and Technology Assessment. Vol. 5034. 2003. p. 112-122.

23. Bruyant, PP.; Gifford, HC.; Gindi, G.; King, MA. Investigation of observer-performance in MAP-EM reconstruction with anatomical priors and scatter correction for lesion detection in ^{67}Ga images. IEEE Nucl. Sci. Symp. Conf. Rec; Oct. 2003; 2003. p. 3166-3169.
24. Tsui BMW, Zhao XD, Gregoriou GK, Lalush DS, Frey EC, Johnston RE, McCartney WH. Quantitative cardiac SPECT reconstruction with reduced image degradation due to patient anatomy. IEEE Trans Nucl Sci. Dec; 1994 41(6):2838–2844.
25. Nelson B, Hayes RL, Edwards CL, Kniseley RM, Andrews GA. Distribution of gallium in human tissues after intravenous administration. J Nucl Med. Jan; 1972 13(1):92–100. [PubMed: 5007973]
26. Ljungberg M, Strand SE. A Monte Carlo program for the simulation of scintillation camera characteristics. Comput Methods Programs Biomed. Aug; 1989 29(4):257–272. [PubMed: 2791527]
27. Pretorius P, King MA, Pan TS, Hutton B. Attenuation correction strategies for multi-energy photon emitters using SPECT. IEEE Trans Nucl Sci. Jun; 1997 44(3):1323–1328.
28. Byrne CL. Accelerating the EMML algorithm and related iterative algorithms by rescaled block-iterative methods. IEEE Trans Image Process. Jan; 1998 7(1):100–109. [PubMed: 18267383]
29. De Pierro AR. A modified expectation maximization algorithm for penalized likelihood estimation in emission tomography. IEEE Trans Med Imag. Mar; 1995 14(1):132–137.
30. Ogawa K, Harata Y, Ichihara T, Kubo A, Hashimoto S. A practical method for position-dependent Compton-scatter correction in single photon emission CT. IEEE Trans Med Imag. Sep; 1991 10(3):408–412.
31. King M, deVries D, Pan TS, Pretorius P, Case J. An investigation of the filtering of TEW scatter estimates used to compensate for scatter with ordered subset reconstructions. IEEE Trans Nucl Sci. Jun; 1997 44(3):1140–1145.
32. Barrett, HH.; Myers, KJ. Foundations of Image Science. Hoboken, NJ: Wiley Interscience; 2004.
33. Wells R, King M, Gifford H, Pretorius P. Single-slice versus multi-slice display for human-observer lesion-detection studies. IEEE Trans Nucl Sci. Jun; 2000 47(3):1037–1044.
34. Nawfel RD, Chan KH, Wagenaar DJ, Judy PF. Evaluation of video gray-scale display. Med Phys. May; 1992 19(3):561–567. [PubMed: 1508090]
35. NIST/SEMATECH e-Handbook of Statistical Methods. [Online]. Available: http://www.itl.nist.gov/div898/handbook/prc/section4/prc47.htm
36. Bruyant, PP.; Gifford, HC.; Gindi, G.; Pretorius, PH.; King, MA. Human and numerical observer studies of lesion detection in Ga-67 images obtained with MAP-EM reconstructions and anatomical priors. IEEE Nucl. Sci. Symp. Conf. Rec; Oct. 2004; 2004. p. 4072-4075.
37. Schillaci O, Danieli R, Manni C, Simonetti G. Is SPECT/CT with a hybrid camera useful to improve scintigraphic imaging interpretation? Nucl Med Commun. Jul; 2004 25(7):705–710. [PubMed: 15208498]
38. Palumbo B, Sivolella S, Palumbo I, Liberati AM, Palumbo R. ^{67}Ga-SPECT/CT with a hybrid system in the clinical management of lymphoma. Eur J Nucl Med Mol Imag. Sep; 2005 32(9): 1011–1017.
39. Chan, C.; Fulton, R.; Feng, DD.; Cai, W.; Meikle, S. An anatomically based regionally adaptive prior for MAP reconstruction in emission tomography. IEEE Nucl. Sci. Symp. Conf. Rec; Nov 2007; 2007. p. 4137-4141.
40. Liao, J.; Qi, J. PET image reconstruction with anatomical prior using multiphase level set method. IEEE Nucl. Sci. Symp. Conf. Rec; Nov. 2007; 2007. p. 4163-4168.
41. Mameuda, Y.; Kudo, H. New anatomical-prior-based image reconstruction method for PET/SPECT. IEEE Nucl. Sci. Symp. Conf. Rec; Nov. 2007; 2007. p. 4142-4148.

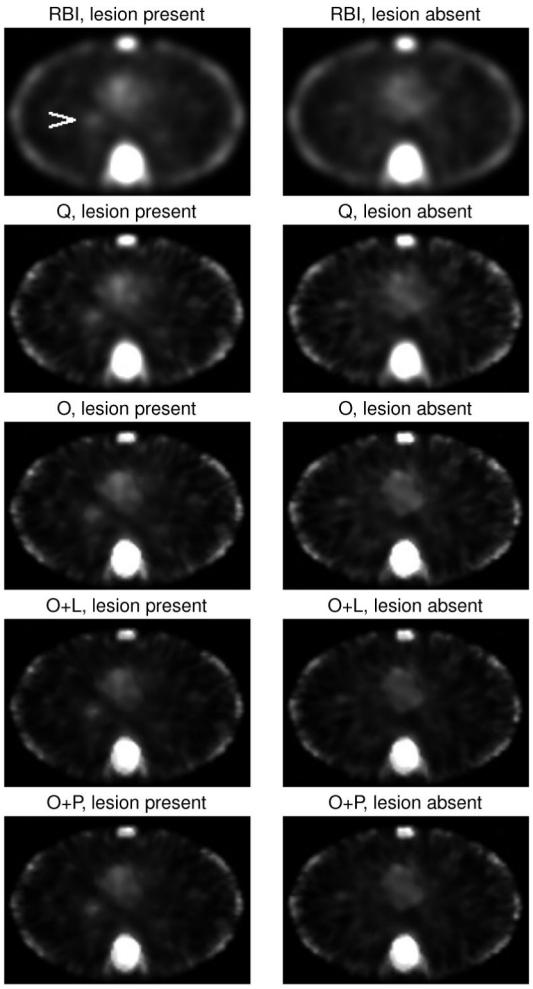

Fig. 1.

Reconstructions of sample lesion-present and matching lesion-absent case reconstructed using several smoothing strategies. Here the lesion, indicated by an arrow, is located far from the organ. The sternum is at the top of the image and the spine at the bottom. The heart is in the center, and ribs are visible at the edge. The prior strength was $\beta = 0.04$. Labels indicating the reconstruction strategy are summarized in Table I.

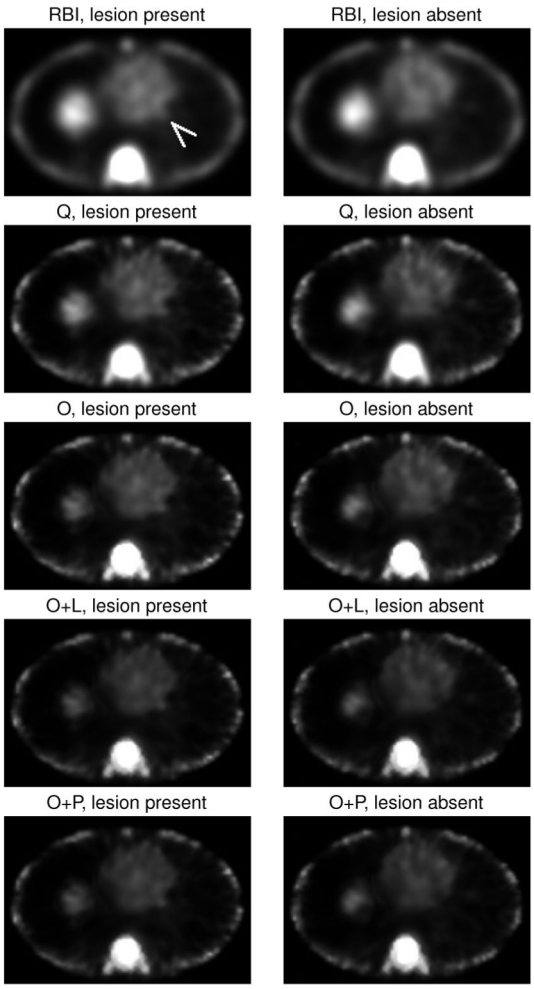

Fig. 2.

Reconstructions of sample lesion-present and matching lesion present case, with the lesion located close to an organ boundary. Arrow indicates lesion location. The heart is in the center of the image, with the liver to its left. The prior strength was $\beta = 0.04$.

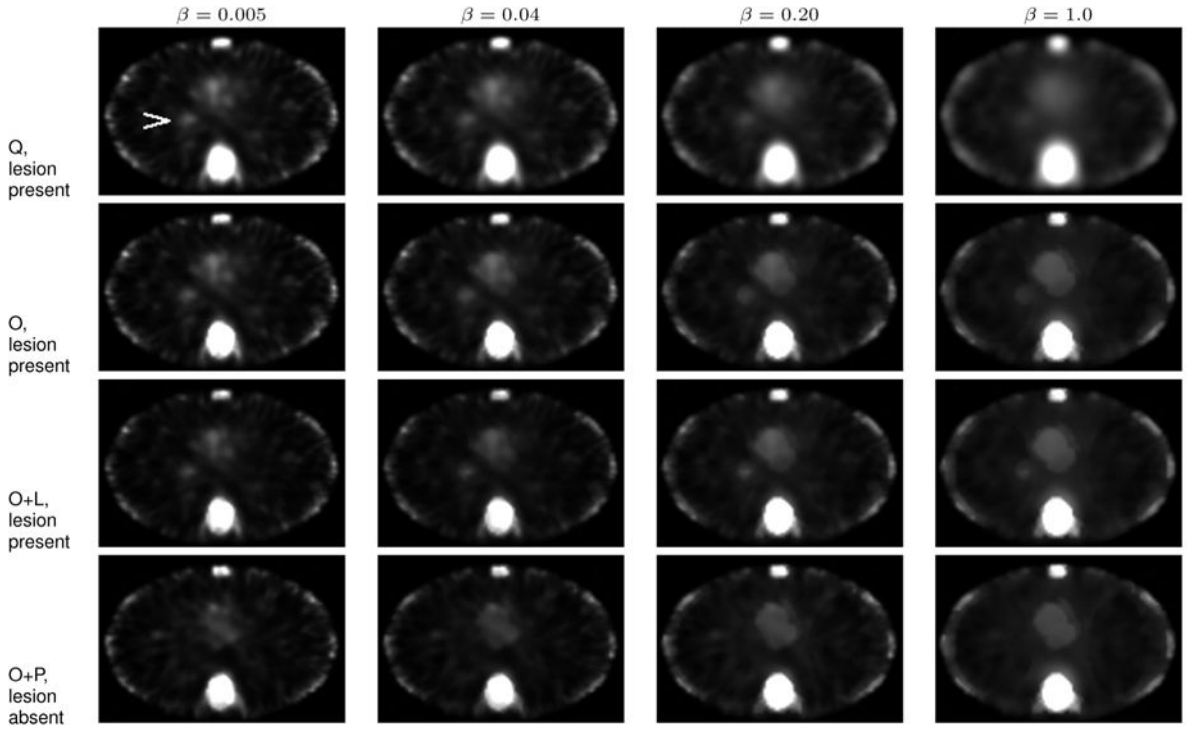

Fig. 3.

Reconstructions of the same lesion-present case shown in Fig. 1 for different values of smoothing strength β. For the matching lesion-absent case strategy O+P is shown. Lesion-present O+P images are not shown as they are identical to the lesion-present O+L. Arrow indicates lesion location.

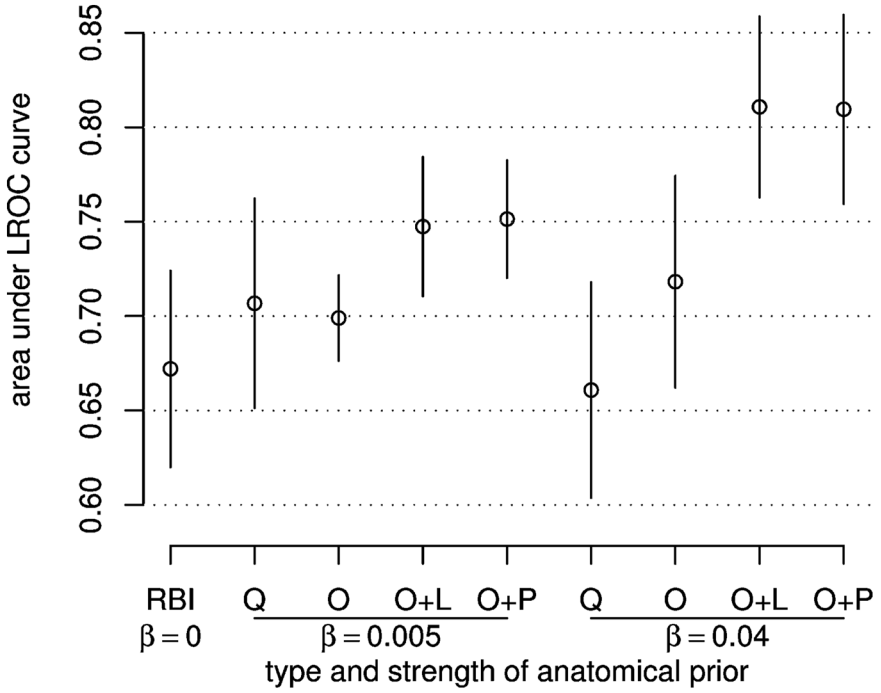

Fig. 4.

Plot showing area under the LROC curve for reconstructions using differing amounts of anatomical information. Circles indicate the mean of five readers, and the bars indicate plus/minus one standard deviation.

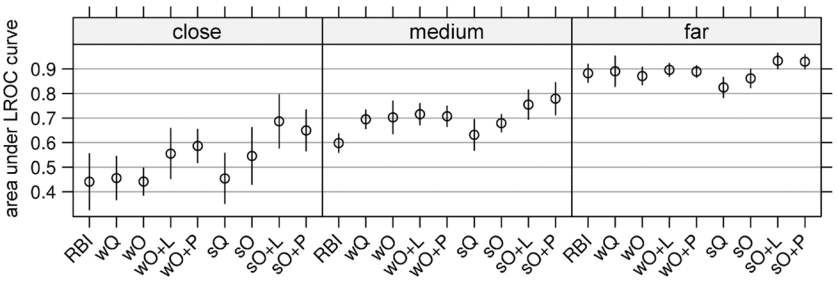

Fig. 5.
Results of partitioning the lesions by distance from organ boundary. Circles represent mean area under the LROC curve of five readers. Bars indicate plus/minus one standard deviation.

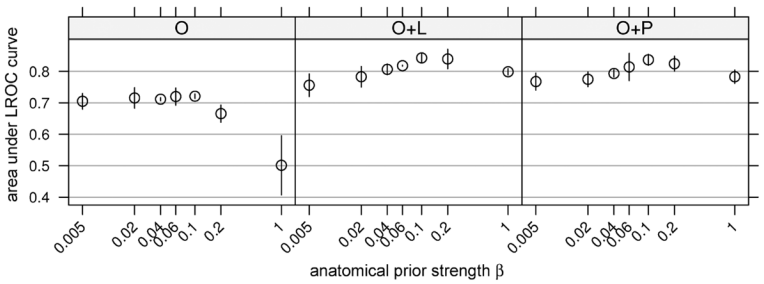

Fig. 6.

Plot showing how area under the LROC curve varies with prior strength β. Note abscissa has a logarithmic scale. Circles represent mean area under the LROC curve of three readers. Bars indicate plus/minus one standard deviation. Note that for β = 0.005 a different set of cases was used than for the other values of β.

TABLE I

Labels Used to Describe Prior Strategies

label	description
RBI	control with no prior
Q	quadratic smoothing, no anatomical boundaries
O	organ boundaries only
O+L	organ + lesion boundaries
O+P	organ + lesion + pseudo-lesion boundaries
w	weak prior ($\beta = 0.005$)
s	strong prior ($\beta = 0.04$)

TABLE II

Results of Tukey's HSD Test to Compare Prior Strategies.

	wQ	wO	wO+L	wO+P	sQ	sO	sO+L	sO+P
RBI	0.529	0.806	**0.003**	**0.002**	0.999	0.183	**0.000**	**0.000**
wQ		1.000	0.325	0.217	0.187	0.999	**0.000**	**0.000**
wO			0.142	0.087	0.403	0.965	**0.000**	**0.000**
wO+L				1.000	**0.000**	0.733	**0.019**	**0.023**
wO+P					**0.000**	0.587	**0.033**	**0.040**
sQ						**0.044**	**0.000**	**0.000**
sO							**0.000**	**0.000**
sO+L								1.000

Bold Indicates Results Significant at the $p < 0.05$ Level. Prior Labels are Summarized in Table I

TABLE III

Results of the Mixture Study

	Rdr 1	Rdr 2	Rdr 3	Mean
control, organ boundaries	0.67	0.66	0.70	0.68
unmixed, organ boundaries	0.70	0.63	0.69	0.67
control, organ+lesion boundaries	0.79	0.75	0.80	0.78
unmixed, organ+lesion boundries	0.79	0.76	0.80	0.78